A GENUINELY MULTIDISCIPLINARY JOURNAL

CHEMPLUSCHEM

CENTERING ON CHEMISTRY

# Accepted Article

**Title:** Directly Synthesized Microporous Bicarbazole-Based Covalent Triazine Frameworks for High-Performance Energy Storage and CO2 Uptake

**Authors:** Mohamed Gamal Mohamed, Ahmed F. M. EL Mahdy, Mahmoud M. M. Ahmed, and Shiao-Wei Kuo



**To be cited as:** *ChemPlusChem* 10.1002/cplu.201900635

**Link to VoR:** http://dx.doi.org/10.1002/cplu.201900635

A Journal of ChemPubSoc Europe

WILEY-VCH

www.chempluschem.org

10.1002/cplu.201900635

WILEY-VCH

FULL PAPER

# Directly Synthesized Microporous Bicarbazole-Based Covalent Triazine Frameworks for High-Performance Energy Storage and Carbon Dioxide Uptake

Mohamed Gamal Mohamed,[a,b] Ahmed F. M. EL-Mahdy,[a,b] Mahmoud M. M. Ahmed,[a] and Shiao-Wei Kuo* [a,c]

**Abstract**

In this study a series of bicarbazole-based covalent triazine frameworks (Car-CTFs) were synthesized under ionothermal conditions from [9,9´-bicarbazole]-3,3´,6,6´-tetracarbonitrile (Car-4CN) in the presence of molten zinc chloride. Thermogravimetric and Brunauer–Emmett–Teller analyses revealed that these Car-CTFs possessed excellent thermal stabilities and high specific surface areas (ca. 1400 $m^2/g$). The electrochemical performances of our Car-CFTs, investigated using cyclic voltammetry, revealed that the highest capacitance was that of the Car-CFT-5-500 sample (545 F/g at 5 mV/s), which also exhibited excellent columbic efficiencies of 96.1% after 8000 cycles at 100 μA/0.5 $cm^2$. The other Car-CFT samples displayed similar efficiencies. Furthermore, based on $CO_2$ uptake measurements, the Car-CTF-5-500 showed the highest $CO_2$ uptake capacities: 3.91 and 7.60 mmol/g at 298 and 273 K, respectively. These results suggest a new simple method for the preparation of CTF materials providing excellent electrochemical and $CO_2$ uptake performance.

**Introduction**

Electric double-layer capacitors are energy storage devices (supercapacitors) that have received much attention from both academia and industry because of their excellent reversibility, high power densities, extra-long cycle lives, discharge/charge ability, and wide window of working temperatures.[1–7] With these outstanding properties, electric double-layer capacitors have been applied in energy storage devices, digital devices, electrical vehicles, and pulsing technologies.[8–11] The energy storage mechanism in supercapacitors depends mainly on the nature of the electrode material; it can be achieved through either Faradaic or non-Faradaic processes. To ensure excellent reversibility and rapid transfer of electrolyte ions at the interface between the electrolyte and the electrode, the electrode materials should possess a hierarchical porous structure and a large electrolyte surface area.[12,13] Accordingly, several advanced porous materials prepared with heteroatom doping, high surface areas, controllable pore size distributions, and excellent electrochemical stability, including covalent triazine-based frameworks (CTFs),[14,15] conjugated microporous polymers (CMPs),[16] and metal organic frameworks (MOFs),[17] are promising candidates for use as electrode materials in energy storage devices.[18] CTFs are a subclass of covalent organic frameworks (COFs); they are high-performance microporous polymeric materials.[19,20] The framework materials of CTFs are rich in nitrogen atoms, have high surface areas with permanent nanopores, and possess excellent chemical and thermal stabilities [because of the triazine units (aromatic C=N linkages) and the absence of weak bonds.[21–23] Recently, CTFs have attracted much attention because of their amazing heteroatom effect and their unique applications in energy storage,[24,25] heterogeneous catalysis,[26] photocatalysis,[27] and gas separation and storage.[28,29] Most CTF materials are semi-crystalline and amorphous because their highly dynamic condensation reactions lead to ultra-strong bonds. CTF framework materials can be prepared using many strategies, including phosphorous pentoxide ($P_2O_5$) catalysis, Friedel–Crafts reactions, superacid catalysis, and ionothermal trimerization of nitrile groups.[30] Thomas et al. were the first to synthesize a series of polymers containing triazine linkages through trimerization of cyano groups under ionothermal conditions, using molten zinc chloride ($ZnCl_2$) as a strong Lewis acid at 400 °C; these polymeric CTF materials displayed high specific surface areas (ca. 790 $m^2/g$).[31]

Dr. M. G. Mohamed, Dr. A. F. M. EL-Mahdy, Dr. M. M. M. Ahmed, Prof. Dr. S.-W. Kuo
[a] Department of Materials and Optoelectronic Science, Center of Crystal Research, National Sun Yat-Sen University, Kaohsiung, Taiwan
E-mail: kuosw@faculty.nsysu.edu.tw
[b] Chemistry Department, Faculty of Science, Assiut University, Assiut 71516, Egypt
[c] Department of Medicinal and Applied Chemistry, Kaohsiung Medical University, Kaohsiung 807, Taiwan

Carbazoles are tricyclic and heterocyclic aromatic amines, first synthesized by Graebe et al.[32] Carbazole (Car) moieties are inexpensive, possess full aromaticity, and are easy to modify; they also exhibit unique photoelectrical properties that have been applied in organic electronics, including photorefractive materials,[33] solar cells,[34] organic light emitting diodes (OLEDs),[35] and fluorescent switches.[36] To tune the electrical and optical properties of a Carbazole unit, substitution can be performed with various functional groups at the nitrogen atom and at the bridged biphenyl units. Furthermore, bicarbazoles, which are formed through N–N coupling of pairs of Car units and feature large dihedral angles (ca. 70°) between the two Car planes, also have great potential for application in OLEDs.[37,38]

In this study, we synthesized [9,9´-bicarbazole]-3,3´,6,6´-tetracarbonitrile (Car-4CN) and used it as a monomer for the preparation of a series of bicarbazole-based nitrogen-rich porous CTFs (Car-CTFs) through trimerization of its nitrile groups in the presence of various mole ratios of $ZnCl_2$ at 400 or 500 °C (**Scheme 1**). We used Fourier transform infrared (FTIR) spectroscopy, solid state $^{13}C$ nuclear magnetic resonance (NMR) spectroscopy, wide-angle X-ray diffraction (WAXD), the Brunauer–Emmett–Teller (BET) method, thermogravimetric analysis (TGA), Raman spectroscopy, and X-ray photoelectron spectroscopy (XPS) to investigate their chemical structures, crystallinity, surface areas, pore size distributions, and microporous structures. Furthermore, we performed electrochemical measurements that revealed their suitability for use as high-performance electrode materials in electrochemical capacitive energy devices. In addition, we did the $CO_2$ uptake measurement for Car-CTFs at 298 and 273 K to examine their $CO_2$ adsorption performance.

**Results and Discussion**

**Synthesis of Car-2Br, Car-4Br, Car-4CN, and Car-CTFs**

As displayed in **Scheme 1**, the monomer Car-4CN was prepared in two steps: (i) carbazole was reacted with NBS in DMF at room temperature to afford Car-2Br, which was reacted with $KMnO_4$ in dry acetone to afford Car-4Br; (ii) Car-4Br then underwent a substitution reaction with CuCN in DMF at 140 °C to give Car-4CN. The chemical structures of Car-2Br, Car-4Br, and Car-4CN were confirmed using FTIR and NMR spectroscopy. **Figure S1** presents the FTIR spectra of Car-2Br, Car-4Br, and Car-4CN. Signals appeared at 3421 $cm^{-1}$ for the N–H stretching of Car-2Br [**Figure S1(a)**]; a signal appeared at 3070 $cm^{-1}$ for C–H stretching in the spectrum of Car-4Br [**Figure S1(b)**], but the signal for the NH group had disappeared. The spectrum of Car-4CN featured a signal at 2220 $cm^{-1}$ for CN stretching [**Figure S1(c)**], confirming its successful synthesis. The $^1H$ NMR spectrum of Car-2Br [**Figure S2(a)**] displays a signal at 10.37 ppm representing the NH unit; this signal was absent in the spectrum of Car-4Br [**Figure S2(b)**]. The $^1H$ NMR spectrum of Car-4CN [**Figure S2(c)**] features signals at 7.32, 7.91, and 9.10 ppm for its aromatic protons. **Figure S3** presents the $^{13}C$ NMR spectra of Car-2Br, Car-4Br, and Car-4CN. **Figure S3(a)** and **3(b)** reveals that the characteristic signal for the carbon nuclei of the C-Br units shifted from 124.32 ppm for Car-2Br to 123.30 ppm for Car-4Br. In addition, in the spectrum of Car-4CN [**Figure S3(c)**] features signals for the **C**-CN and CN units at 121.81 and 127.59 ppm, respectively. These FTIR and NMR spectral data confirmed the successful synthesis and high purity of the Car-4CN monomer. We employed an ionothermal method to react the monomer Car-4CN with various amounts of molten $ZnCl_2$ at 400 or 500 °C to prepare four kinds of Car-CTFs, as presented in **Scheme 1** and **Table 1**. We used FTIR spectroscopy and DSC to monitor the trimerizations of the cyano groups of Car-4CN at temperatures ranging room temperature to 400 °C, as depicted in **Figure 1**. The FTIR spectra in **Figure 1(A)** reveal that the characteristic absorption band at 2220 $cm^{-1}$ for CN stretching remained for the reactions performed at 25 to 370 °C. When the reaction temperature was 400 °C, however, the typical band for the cyano groups disappeared from the spectrum of Car-CTF-5-400, with two characteristics bands at 1565 and 1360 $cm^{-1}$ present for triazine rings. In the DSC curve of Car-4CN [**Figure 1(B)**], a maximum exothermic peak appeared at 305 °C with a reaction heat of 148.5 J $g^{-1}$ for the cyclotrimerization reaction of nitrile groups. When the reaction temperature was 400 °C, the maximum exothermic peak was completely absent from the DSC curve of Car-CTF-

10.1002/cplu.201900635




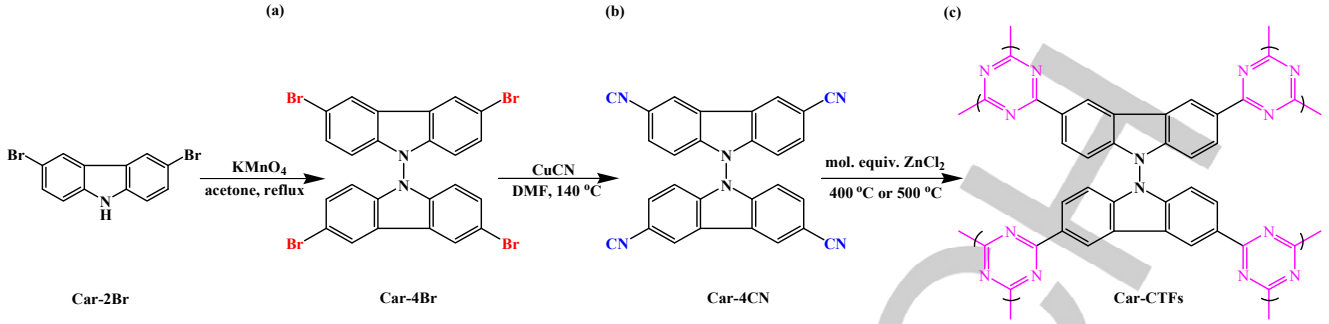


**Scheme 1.** Synthesis of (a) Car-4Br, (b) Car-4CN, and (c) the Car-CTFs.

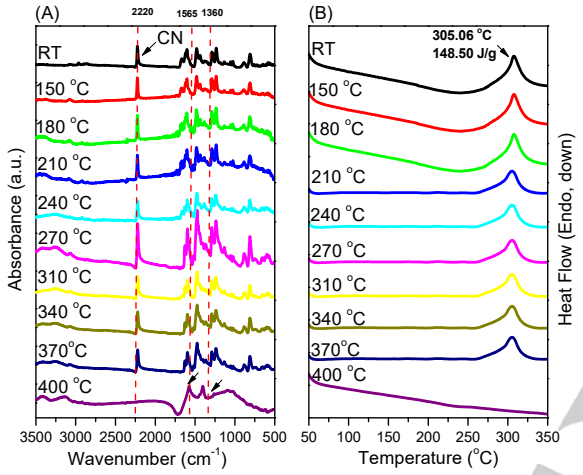


**Figure 1.** (A) FTIR spectra and (B) DSC thermograms of Car-4CN after thermal treatment at various temperatures from 25 to 400 °C.

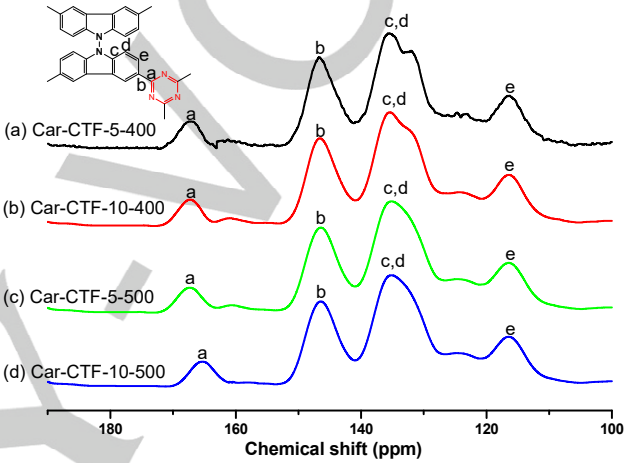


**Figure 2.** Solid state $^{13}$CCP/MAS NMR spectra of (a) Car-CTF-5-400, (b) Car-CTF-10-400, (c) Car-CTF-5-500, and (d) Car-CTF-10-500.

5-400.[42] These DSC and FTIR spectral data confirmed the complete trimerization of the nitrile groups in Car-CTF-5-400 at 400 °C.

**Figure S4** displays FTIR spectra of Car-4CN and the four obtained Car-CTFs. A signal representing nitrile groups (typically at 2220 cm$^{-1}$) was absent in the spectra of all of the Car-CTFs [**Figures S4(b-e)**], while the two typical absorption bands for triazine rings (at 1565 and 1365 cm$^{-1}$) were present, confirming the successful trimerization of the cyano groups when performing the reactions using molten $ZnCl_2$ at 400 and 500 °C.[41] Powder X-ray diffraction patterns (**Figure S5**) revealed that all of the synthesized Car-CTFs were amorphous, with no obvious signals for crystalline peaks. Solid state $^{13}$C CP/MAS NMR spectroscopy confirmed the formation of the triazine rings in the Car-CTF materials (**Figure 2**), with the major signals appearing at 168.28, 146.58, 135.82, and 116.24 ppm for the carbon nuclei of the triazine rings (-CAr=N-) and other aromatic carbon atoms in the Car moieties.[42,43,44]

We used TGA (heating rate: 20 °C min$^{-1}$; from 25 to 800 °C) to investigate the thermal stability of the Car-CTF polymeric materials under a $N_2$ atmosphere (**Figure 3(A)**, **Table 1**). According to the TGA analyses of Car-CTF-5-400 and Car-CTF-10-400, which were both prepared at 400 °C, the former featured a higher degradation temperature $T_{d10\%}$ (471 °C) and char yield (65%) when compared with those of the latter (465 °C, 63%), as well as those of the Car-4CN monomer (361.8 °C, 26%). In comparison, Car-CTF-5-500 and Car-CTF-10-500 began to decompose at 556 and 527 °C, respectively, with char yields of 74 and 66%, respectively, indicating that these framework materials had superior thermal stability.[45] **Figure 3(B)** presents the Raman spectra of our Car-CTFs, in the range from 1000 to 1900 cm$^{-1}$. All the synthesized Car-CTF framework materials exhibited two strong bands namely, the D- and G-bands representing the major graphitic-carbonized structure. These two bands corresponded to the second-order Raman scattering (with $sp^3$ hybridization) and first-order Raman scattering (with $sp^2$ hybridization) of

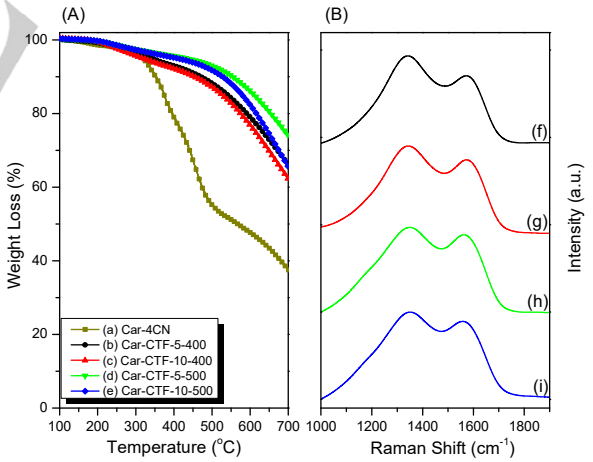


**Figure 3.** (A) TGA curves and (B) Raman spectra of Car-4CN, Car-CTF-5-400, Car-CTF-10-400, Car-CTF-5-500, and Car-CTF-10-500.

the graphitic carbon atoms, respectively. The D-bands appeared at 1354.0, 1354.4, 1349.0, and 1347.4 cm$^{-1}$ for Car-CTF-5-400, Car-CTF-10-400, Car-CTF-5-500, and Car-CTF-10-500, respectively, while their G-bands appeared at 1577.0, 1581.5, 1573.8, and 1580.9 cm$^{-1}$, respectively. The positions of the G-bands were closer to that of graphene (1581 cm$^{-1}$) for both Car-CTF-10-400 and Car-CTF-10-500, suggesting that both Car-CTF-10-400 and Car-CTF-10-500 provided a better graphenoid structure than Car-CTF-5-400 and Car-CTF-5-500.

**Table 1** TGA results, BET parameters, Raman spectra and CV results of the synthesized Car-CTFs

| Sample | Car-4CN/$ZnCl_2$ | $T_{d10\%}$ (°C) | Char Yield (%) | $S_{BET}$ ($m^2$/g) | Pore size (nm) | Pore Volume ($cm^3$/g) | Raman ($I_D/I_G$) | CV (F/g) |
|---|---|---|---|---|---|---|---|---|
| Car-CTF-5-400 | 1:5 | 471 | 65 | 910.7 | 2.00 | 0.45 | 2.3 | 420 |
| Car-CTF-10-400 | 1:10 | 465 | 63 | 1248.6 | 2.10 | 0.65 | 2.5 | 388 |
| Car-CTF-5-500 | 1:5 | 556 | 74 | 1410.7 | 2.33 | 0.82 | 2.6 | 545 |
| Car-CTF-10-500 | 1:10 | 527 | 66 | 1334.4 | 2.89 | 0.96 | 2.6 | 470 |

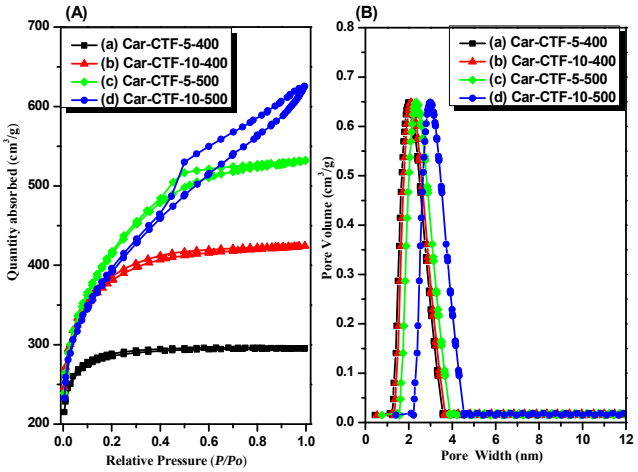


**Figure 4.** (A) $N_2$ adsorption/desorption isotherms and (B) pore size distributions of (a) Car-CTF-5-400, (b) Car-CTF-10-400, (c) Car-CTF-5-500, and (d) Car-CTF-10-500.

furthermore, this data also reveals lower Fermi energy levels and smaller band gaps for Car-CTF-10-400 and Car-CTF-10-500.[46] The $I_D/I_G$ ratios for Car-CTF-5-400, Car-CTF-10-400, Car-CTF-5-500, and Car-CTF-10-500 were 2.3, 2.5, 2.6, and 2.6, respectively, suggesting a less-defected structure for Car-CTF-5-400 relative to the others.[47,48]

**BET, TEM, and XPS Analyses of Car-CTFs**

**Figure 4** and **Table 1** present the results of $N_2$ adsorption/desorption experiments performed at 77 K, to investigate the porosity properties and pore size distributions of all the synthesized Car-CTFs. In **Figure 4(A)**, both Car-CTF-5-400 and Car-CTF-10-400 display typical reversible isotherms at low relative pressure ($P/P_o$), with steep increases in $N_2$ adsorption in the low-$P/P_o$ region, indicating that both materials possessed microporous characteristics, with high specific surface areas of 910 and 1248 $m^2$/g, respectively, and pore volumes of 0.457 and 0.656 $cm^3$/g, respectively. When the amount of molten $ZnCl_2$ and the reaction temperature for the trimerization of the nitrile group both increased, the surface area and porosity of the Car-CTF materials also increased.[31,45] Car-CTF-5-500 and Car-CTF-10-500 provided high surface areas of 1410 and 1334 $m^2$/g, respectively, with type IV isotherms and associated $H_2$ hysteresis for a microporous and mesoporous materials, and pore volumes of 0.823 and 0.966 $cm^3$/g, respectively. We attribute the higher surface area and porosity of Car-CTF-5-500, relative to those of Car-CTF-5-400, Car-CTF-10-400, and Car-CTF-10-500, to the existence of large extra defects in the Car-CTF-5-500 structure and the formation the close-packed nanoparticles inside Car-CTF-5-500 at higher temperature.[42,49,50] The pore size distributions in the Car-CTF framework materials were determined and calculated according to nonlocal density functional theory (NL-DFT) [**Figure 4(B)** and **Table 1**]. The pore sizes for Car-CTF-5-400, Car-CTF-10-400, Car-CTF-5-500, and Car-CTF-10-500 were 2.00, 2.10, 2.33, and 2.89 nm, respectively. TEM images (**Figure S6(a-d)**) of the Car-CTF materials revealed that Car-CTF-5-400, Car-CTF-10-400, Car-CTF-5-500 and Car-CTF-10-500 possessed porous structures. The SEM images in **Figure S7** reveal that all the Car-CTFs were prepared as irregular small and large particles of various sizes (>1 μm).[44]

XPS survey spectra of the Car-CTFs (**Figure S8)** featured three distinct peaks centered at 284, 400, and 530 eV, representing (i) the carbon atoms of the aromatic rings in the polymeric frameworks, (ii) the N 1s orbitals of the C–N bonds in the triazine units, and (iii) the O 1s orbitals of absorbed water and oxygen, respectively. These three peaks were

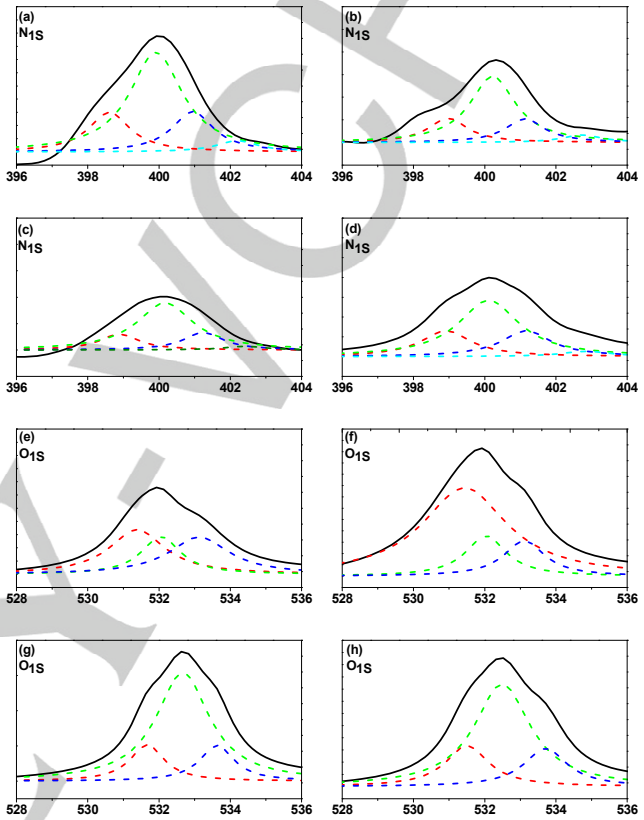


**Figure 5**. XPS spectra (a–d) N1s and (e–h) O1s orbitals of (a, e) Car-CTF-5-400, (b, f) Car-CTF-10-400, (c, g) Car-CTF-5-500, and (d, h) Car-CTF-10-500.

consistent with the successful synthesis of the CTF frameworks. To better understand the types of N and O species in the Car-CTF framework materials, we obtained XPS fitting curves for the $N_{1s}$ and $O_{1s}$ orbitals (**Figure 5**, **Table 2**). As revealed in **Figures 5(a-d)**, three major types of N species were present on the surfaces of the Car-CTFs. We assign the three peaks centered at 398.7, 400.1, and 401.2 eV to the hexagonal pyridinic N atoms in triazine rings, pyrrolic N atoms, and quaternary N atoms, respectively. The pyridinic and pyrrolic N species were the most preferentially formed in the Car-CTF materials, according to quantitative analysis. The O 1s spectra [**Figures 5(e-g)**] were fitted into three peaks at 531, 532, and 533 eV; the first corresponding to polarized C–O bonds (for C=O and phenolic OH groups) and the other two ascribed to absorbed oxygen and water.[5,47,51,52]

**Electrochemical performance and $CO_2$ uptake properties**

We recorded CV curves for the four Car-CTF samples in 1.0 M aqueous KCl within the range from -1.0 to 1.0 V at 5–200 mV/s. Although Car derivatives are well known and have been studied previously for various electrochemical applications (e.g., supercapacitors,[53,54] oxygen reduction applications,[55] lithium sulfur batteries,[56] hydrogen production[57]), to the best of our knowledge such inactivated structures have not been examined yet. **Figure 6** presents CV curves of these four Car-CTFs, revealing hybrid-type supercapacitor performance with major electric

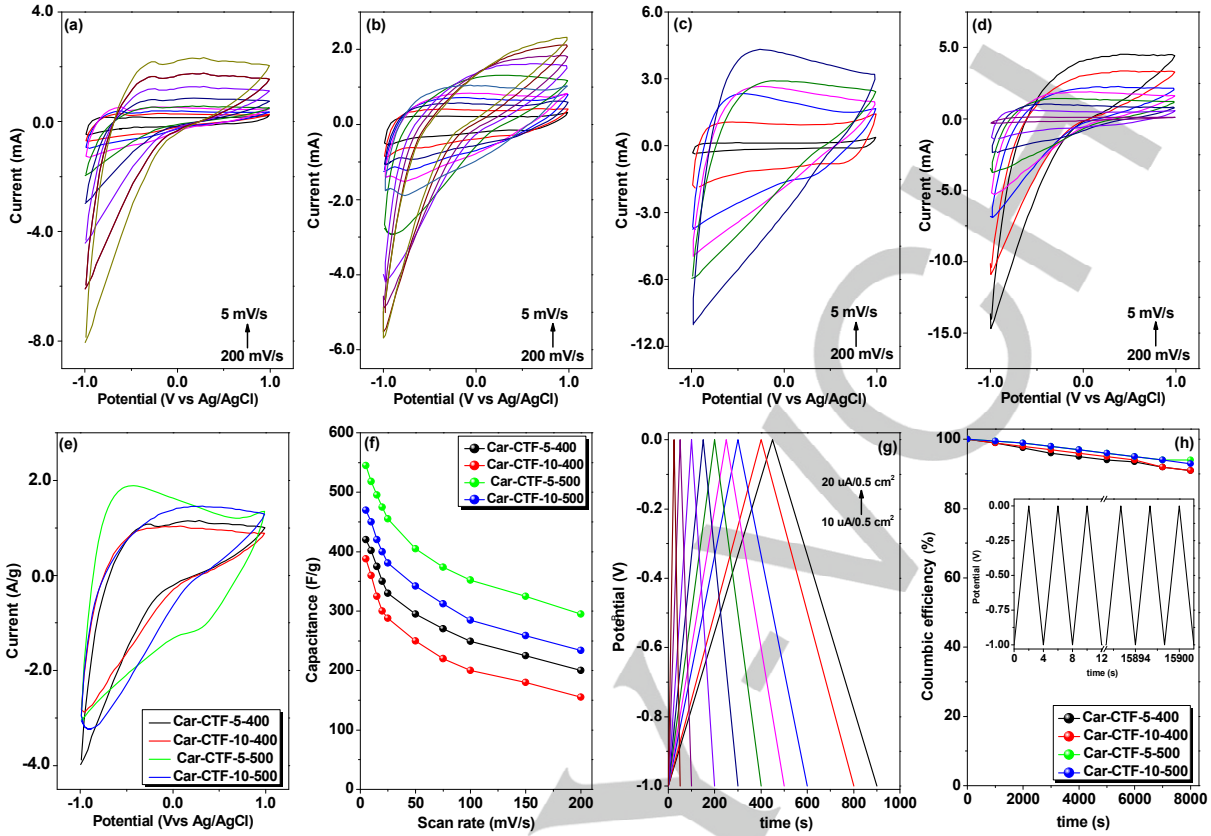


**Figure 6.** (a–d) Cyclic voltammetry curves of (a) Car-CTF-5-400, (b) Car-CTF-10-400, (c) Car-CTF-5-500, and (d) Car-CTF-10-500. (e) Comparison of the CV at 50 mV/s (f) Capacitance plotted with respect to the scan rate. (g) Charge/discharge performance of Car-CTF-5-500 at various currents. (h) Columbic efficiencies of the Car-CTFs at 100 μA/0.5 $cm^2$.

**Table 2** Area fractions of signals in N 1s and O 1s spectra, based on curve-fitting data from **Figure 5**

| Sample | N species | | | O species | | |
|---|---|---|---|---|---|---|
| | N-6 | N-5 | N-Q | C– O | C-OH | $H_2O$ |
| Car-CTF-5-400 | 57.89 | 18.26 | 23.84 | 39.79 | 24.05 | 36.16 |
| Car-CTF-10-400 | 18.30 | 58.14 | 23.56 | 69.65 | 16.11 | 14.24 |
| Car-CTF-5-500 | 15.52 | 63.68 | 20.79 | 69.70 | 15.25 | 15.05 |
| Car-CTF-10 500 | 20.80 | 54.20 | 25.00 | 62.54 | 19.26 | 18.20 |

double layer capacitor (EDLC) and minor pseudocapacitor (PC) performance within the investigated range for all the carbonized samples (**Table 1**). Interestingly, our previously reported hollow microspherical Car-based framework displayed efficient PC performance together with EDLC when investigated within the range from 0.0 to 0.6 V, due to the presence of the triazine moieties.[58] In this present study, the reaction with $ZnCl_2$ produced more efficient EDLC performance, rather than the PC effect, possibly because of structural reformation. In particular, the reaction with $ZnCl_2$ formed a new carbon framework with pyridinic N atoms like those found in N-doped carbon materials. Therefore, the EDLC shapes were more dominant for all the Car-CTFs. The EDLC shapes for all Car-CTFs were like those of graphene composites.[59] In addition, all Car-CTFs functioned as hybrid capacitors with both EDLC and PC characteristics, due to the major hybridizations of the graphitic carbon structure with different groups, as revealed in the XPS data. In addition, the capacitance data obtained from the CV curves [**Figure 6(f)**] revealed that the capacitances for Car-CTF-5-400, Car-CTF-10-400, Car-CTF-5-500, and Car-CTF-10-500 reached 420, 388, 545 and 470 F/g, respectively. Thus, Car-CTF-5-500 exhibited magnificent storage capacitance, possibly because of its uniform carbon structure. These enhanced capacitance performances are higher than other investigated carbazole-related structures even the heating temperature was 500 °C only. A comparison study is included in (**Table S1**). These results also could be attributed to the surface area increase upon reaction with $ZnCl_2$ at higher temperature suggesting minor oxidations and hybridizations with structural reformations. This also can enrich the PC performance. In addition, we examined the CD performance for Car-CTF-5-500 over the range of -1.0 to 0.0 V, using currents of 10, 11, 12, 14, 15, 16, 17, 18, 19 and 20 μA/$cm^2$ [**Figure 6(g)**]. The CD curves reveal typical symmetrical CD patterns with a negligible internal resistance drop, indicating that the hybridization did not induce further resistive structure. Furthermore, we evaluated the columbic efficiencies under CD procedures at 100 μA/0.5 $cm^2$ over 8000 cycles. For Car-CTF-5-400, Car-CTF-10-400, Car-CTF-5-500, and Car-CTF-10-500, the average columbic efficiencies were 94.0, 96.0, 96.1, and 93%, respectively. This indicates the efficient durability of the produced materials under sever conditions. This performance indicates that these materials can be used in industrial applications.

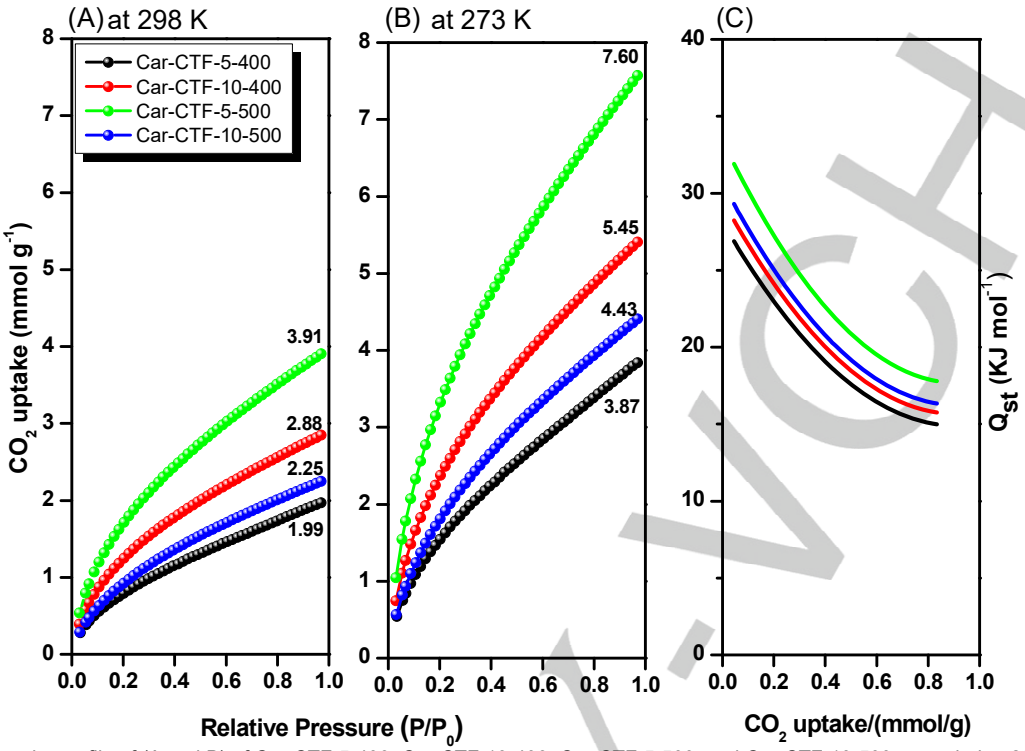


**Figure 7**. $CO_2$ uptake profile of (A and B) of Car-CTF-5-400, Car-CTF-10-400, Car-CTF-5-500, and Car-CTF-10-500, recorded at 298 K and 273 K and (C) $CO_2$ isosteric heats of adsorption of Car-CTF-5-400, Car-CTF-10-400, Car-CTF-5-500, and Car-CTF-10-500.

Because of the high surface area, microporous structure and the unique N-heteroatom framework of the all synthesized Car-CTFS, the $CO_2$ adsorption isotherms were done at 298 and 273 K, as displayed in **Figure 7(A) and (B)**, respectively. As shown in **Figure 7**, the Car-CTF-10-400 and Car-CTF-5-500 exhibiting a higher $CO_2$ uptake capacity of 2.88, 3.91 mmol/g at 298 K and 5.45, 7.60 mmol/g at 273 K, which attributed to presence the highest nitrogen content inside these materials (based on XPS results). While, Car-CTF-5-400 and Car-CTF-10-500 displayed $CO_2$ uptake capacities of 1.99 and 2.25 mmol/g at 298 and 3.87 and 4.43 mmol/g at 273 K. More interestingly, the synthesized Car-CTF-5-500 [**Figure 7(A)**] displays much higher $CO_2$ uptake capacity of 3.91 mmol/g at 298 K compared with other previous synthesized CTFs at the same temperature such as CTF-0 (1.54-2.34 mmol/g),[49] CTF-DCN-500 (2.70 mmol/g),[42] CTF-1 (2.77 mmol/g),[28] CTF-20-400 (3.48 mmol/g)[45] and PCTF-1 to 3 (2.02-3 mmol/g).[60] Also, we have calculated the isosteric heat of adsorption ($Q_{st}$) from the $CO_2$ uptake data recorded at 298 and 273 K by using the Clausius-Clapeyron equation [**Figure 7(C)**]. At low coverage of $CO_2$, the Car-CTF-5-400, Car-CTF-10-400, Car-CTF-5-500, and Car-CTF-10-500 provided values of $Q_{st}$ of 26.79, 27.94, 31.74 and 29.47 kJ/mol, respectively. These results indicate that these Car-CTFs materials have strong interactions with $CO_2$ molecules and their Qst values are similar to the $Q_{st}$ value of $CO_2$ uptake on activated carbons.[61-64] CV and $CO_2$ uptake measurements, suggest the potential performance of Car-CTFs in energy storage and gas storage applications.

## Conclusions

We have synthesized a new series of conductive bicarbazole-based CTFs through the trimerization of Car-4CN in the presence of molten zinc chloride. All the four synthesized microporous Car-CTFs exhibited high thermal stability and high specific surface areas (>1400 $m^2/g$). Moreover, the electrochemical performances of each Car-CTF revealed highly stable efficiency, with the highest capacitance being that for Car-CTF-5-500: 545 F/g at 5 mV/s. In addition, all synthesized Car-CTFs possess microporous nature, high surface area, and the unique N-heteroatom framework. Thus. all synthesized Car-CTFS exhibiting high $CO_2$ uptake capacities of 1.99, 2.88, 3.91 and 2.25 mmol/g for Car-CTF-5-400, Car-CTF-10-400, Car-CTF-5-500, and Car-CTF-10-500 at 298 K, respectively, and these values of $CO_2$ uptake were higher than that of numerous synthesized CTFs at 298 K such as CTF-1, CTF-0, CTF-20-400, and CTF-DCN-500. We believe that this new synthetic approach provides new types of CTFs materials with good thermal stability, high surface area, electrochemically stable triazine frameworks, and excellent carbon dioxide capture.

## Experimental Section

### Materials

Carbazole (98%), dichloromethane (DCM), ethanol, methanol, anhydrous magnesium sulfate ($MgSO_4$), hydrochloric acid (37%), and *N*-bromosuccinimide (NBS) were purchased from Acros. Potassium permanganate ($KMnO_4$), ethylenediamine (99%), tetrahydrofuran (THF), *N*,*N*-dimethylformamide (DMF), acetone, and copper(I) cyanide (CuCN) was purchased from Sigma–Aldrich.

### 3,6-Dibromo-9*H*-carbazole (Car-2Br)[39,40]

In a 500-mL two-neck bottle, a solution of NBS (5.00 g, 28.0 mmol) in anhydrous DMF (25 mL) was added dropwise over 1 h to a solution of carbazole (2.34 g, 14.0 mmol) in DCM (140 mL). The mixture was stirred for 24 h at 25 °C and then washed three times with $H_2O$. The DCM phase was dried (anhydrous $MgSO_4$), filtered, and concentrated using a rotary evaporator. The white powder was dissolved in dry acetone (25 mL) and precipitated with hexane (150 mL). The precipitate was filtered off and dried under vacuum at 50 °C to afford a white solid (3.6 g). $^1$H NMR ($CDCl_3$, 25 °C, 500 MHz): δ = 7.31 (d, *J* = 8.6 Hz, 2H), 7.52 (d, *J* = 8.6 Hz, 2H), 8.13 (d, *J* = 1.9 Hz, 2H), 10.37 (s, 1 H). $^{13}$C NMR ($CDCl_3$, 25 °C, 125 MHz): δ = 139.40, 129.26, 124.45, 113.07, 112.32.

### 3,3´,6,6´-Tetrabromo-9,9´-bicarbazole (Car-4Br)[39,40]

In a 250-mL one-neck bottle, a solution of 3,6-dibromocarbazole (3.00 g, 9.23 mmol) and $KMnO_4$ (4.38 g, 27.9 mmol) in acetone (80 mL) was heated under reflux at 50 °C for 6 h. Distilled water (50 mL) was added and then the mixture stirred for 2 h at 25 °C. The aqueous phase was extracted three times with DCM (50 mL). The combined organic phases were dried (anhydrous $MgSO_4$) and concentrated under reduced pressure to give a white powder (6.92 g). $^1$H NMR ($CDCl_3$, 25 °C, 500 MHz): δ = 8.26 (d, 4H), 7.47 (d, *J* = 10.4 Hz, 4H), 6.74 (d, *J* = 8.6 Hz, 4H). $^{13}$C NMR ($CDCl_3$, 25 °C, 500 MHz): δ = 139.34, 131.26, 124.49, 123.14, 115.56, 110.82.

### Car-4CN

A mixture of Car-4Br (2.58 g, 4.00 mmol) and CuCN (9.69, 108 mmol) in dry DMF (100 mL) in a 250-mL two-neck flask was heated under reflux for

3 days at 140 °C under a $N_2$ atmosphere. After cooling to room temperature, the mixture was filtered and the solution poured into a mixture of cold water (75 mL) and ethylenediamine (4 mL), and then the mixture was stirred for 2 h at 25 °C. The precipitate was filtrated off and washed several times with water and MeOH to afford a white powder (1.24 g). FTIR (KBr, $cm^{-1}$): 3070 (CH stretching), 2220 (CN stretching). $^1H$ NMR (DMSO-$d_6$, 25 °C, 500 MHz): δ = 7.32 (d, *J* = 8 Hz, 4H), 7.91 (d, *J* = 8 Hz, 4H), 9.10 (s, 4H). $^{13}C$ NMR (DMSO-$d_6$, 25 °C, 125 MHz): δ = 141.95, 132.20, 127.59, 121.81, 119.74, 110.99, 105.63.

**Car-CTFs**

A mixture of Car-4CN (200 mg, 0.460 mmol) and anhydrous $ZnCl_2$ [ranging from 32 mg (2.32 mmol) to 63 mg (4.63 mmol)] was charged in an ampoule, as displayed in **Scheme 1**. Under a $N_2$ atmosphere, the ampoule was heated to 400 or 500 °C at a heating rate of 5 °C $min^{-1}$, and then maintained at that temperature for 72 h. After cooling to room temperature, the obtained black solid was stirred in a solution of 1 M HCl and water for 24 h to remove unreacted metal salt ($ZnCl_2$), respectively. The resulting black solid (Car-CTF-5-400, Car-CTF-10-400, Car-CTF-5-500, or Car-CTF-10-500; **Scheme 1** and **Table 1**) was washed sequentially with THF, acetone, and MeOH and then dried under vacuum at 120 °C for 48 h.

**Acknowledgments**

This study was supported financially by the Ministry of Science and Technology, Taiwan, under contracts MOST 106-2221-E-110-067-MY3, 105-2221-E-110-092-MY3, and 108-2218-E-110-013 -MY3.

**Keywords**: Carbazole; carbon dioxide capture; covalent triazine frameworks; microporous polymers; supercapacitors.

**References**

[1] T. Quan, N. Goubard-Bretesché, E. Härk, Z. Kochovski, S. Mei, N. Pinna, M. Ballauff and Y. Lu, *Chem. Eur. J.* **2019**, *25*, 4757-4766..
[2] J. Bi, B. Xu, L. Sun, H. Huang, S. Fang, L. Li, L. Wu, *ChemPlusChem* **2019**, 84, 1149-1154.
[3] J. Tang, T. Wang, R. R. Salunkhe, S. M. Alshehri, V. Malgras, Y. Yamauchi, *Chem. Eur. J.* **2015**, *21*, 17293-17298.
[4] N. L. Torad, R. R. Salunkhe, Y. Li, H. Hamoudi, M. Imura, Y. Sakka, C.-C. Hu, Y. Yamauchi, *Chem. Eur. J.* **2014**, *20*, 7895-7900.
[5] P. Zhang, J. Zhang and S. Dai, *Chem. Eur. J.* **2017**, *23*, 1986-1998.
[6] H. Nishihara, T. Kyotani, *Adv. Mater.* **2012**, *24*, 4473-4498.
[7] H. Zhang , M. Zhang , P. Lin , V. Malgras, J. Tang , S. M. Alshehri, Y. Yamauchi , S. Du, J. Zhang, *Chem. Eur. J.* **2016**,*22*, 1141-1145.
[8] L. L. Zhang, X. Zhao, *Chem. Soc. Rev.* **2009**, *38*, 2520-2531.
[9] M. Kim, P. Puthiaraj, Y. Qian, Y. Kim, S. Jang, S. Hwang, E. Na, W.-S. Ahn, S. E. Shim, *Electrochim. Acta* **2018**, *284*, 98-107.
[10] K. Zhang, L. L. Zhang, X. Zhao, J. Wu, *Chem. Mater.* **2010**, *22*, 1392-1401.
[11] G. A. Snook, P. Kao, A. S. Best, *J. Power Sources* **2011**, *196*, 1-12.
[12] R. Kötz, M. Carlen, *Electrochim. Acta* **2000**, *45*, 2483-2498.
[13] A. F. El-Mahdy, Y. H. Hung, T. H. Mansoure, H. H. Yu, T. Chen, S. W. Kuo, *Chem. Asian J.* **2019**, *14*, 1429-1435.
[14] L. Hao, B. Luo, X. Li, M. Jin, Y. Fang, Z. Tang, Y. Jia, M. Liang, A. Thomas, J. Yang, *Energy Environ. Sci.* **2012**, *5*, 9747-9751.
[15] S. Hug, M. B. Mesch, H. Oh, N. Popp, M. Hirscher, J. Senker, B. V. Lotsch, *J. Mater. Chem. A* **2014**, *2*, 5928-5936.
[16] T. Zhu, Q. Yu, L. Ding, T. Di, T. Zhao, T. Li, L. Li, *Green Chem.* **2019**, *21*, 2326-2333.
[17] C.-C. Chueh, C.-I. Chen, Y.-A. Su, H. Konnerth, Y.-J. Gu, C.-W. Kung, K. C.-W. Wu, *J. Mater. Chem. A* **2019**, *7*, 17079-27095.
[18] X. Jiang, P. Wang, J. Zhao, *J. Mater. Chem. A* **2015**, *3*, 7750-7758.
[19] P. Kuhn, A. Forget, D. Su, A. Thomas, M. Antonietti, *J. Am. Chem. Soc.* **2008**, *130*, 13333-13337.
[20] A. F. El-Mahdy, C.-H. Kuo, A. Alshehri, C. Young, Y. Yamauchi, J. Kim, S.-W. Kuo, *J. Mater. Chem. A* **2018**, *6*, 19532-19541.
[21] S. Ren, R. Dawson, A. Laybourn, J.X. Jiang, Y. Khimyak, D. J. Adams, A. I. Cooper, *Polymer Chem.* **2012**, *3*, 928-934.
[22] S. Hug, L. Stegbauer, H. Oh, M. Hirscher, B. V. Lotsch, *Chem. Mater.* **2015**, *27*, 8001-8010.
[23] L. Tao, F. Niu, C. Wang, J. Liu, T. Wang, Q. Wang, *J. Mater. Chem. A* **2016**, *4*, 11812-11820.
[24] J. Liu, P. Lyu, Y. Zhang, P. Nachtigall, Y. Xu, *Adv. Mater.* **2018**, *30*, 1705401.
[25] F. Xu, S. Yang, G. Jiang, Q. Ye, B. Wei, H. Wang, *ACS App. Mater. Interf.* **2017**, *9*, 37731-37738.
[26] P. Puthiaraj, Y.-R. Lee, S. Zhang, W.-S. Ahn, *J. Mater. Chem. A* **2016**, *4*, 16288-16311.
[27] L. Guo, Y. Niu, H. Xu, Q. Li, S. Razzaque, Q. Huang, S. Jin, B. Tan, *J. Mater. Chem. A* **2018**, *6*, 19775-19781.
[28] Y. Zhao, K. X. Yao, B. Teng, T. Zhang, Y. Han, *Energy Environ. Sci.* **2013**, *6*, 3684-3692.
[29] W. Yu, S. Gu, Y. Fu, S. Xiong, C. Pan, Y. Liu, G. Yu, *J. Catal.* **2018**, *362*, 1-9.
[30] M. Liu, L. Guo, S. Jin, B. Tan, *J. Mater. Chem. A* **2019**, *7*, 5153-5172.
[31] P. Kuhn, M. Antonietti, A. Thomas, *Angew. Chem. Int. Ed.* **2008**, *47*, 3450-3453.
[32] C. Glaser, *Berichte der deutschen chemischen Gesellschaft* **1872**, *5*, 982-982.
[33] Y. Zhang, T. Wada, H. Sasabe, *J. Mater. Chem.* **1998**, *8*, 809-828.
[34] S. Wakim, S. Beaupré, N. Blouin, B.-R. Aich, S. Rodman, R. Gaudiana, Y. Tao, M. Leclerc, *J. Mater. Chem.* **2009**, *19*, 5351-5358.
[35] B. Wex, B. R. Kaafarani, *J. Mater. Chem. C* **2017**, *5*, 8622-8653.
[36] P. Xue, J. Sun, P. Chen, P. Wang, B. Yao, P. Gong, Z. Zhang, R. Lu, *Chem. Comm.* **2015**, *51*, 10381-10384.
[37] X.-Y. Liu, Y.-L. Zhang, X. Fei, L.-S. Liao, J. Fan, *Chem. Eur. J.* **2019**, *25*, 4501-4508.
[38] Y. Yuan, H. Huang, L. Chen, Y. Chen, *Macromolecules* **2017**, *50*, 4993-5003.
[39] S. Feng, H. Xu, C. Zhang, Y. Chen, J. Zeng, D. Jiang, J.-X. Jiang, *Chem. Comm.* **2017**, *53*, 11334-11337.
[40] Q. Mu, J. Liu, W. Chen, X. Song, X. Liu, X. Zhang, Z. Chang, L. Chen, *Chem. Eur. J.* **2019**, *25*, 1901-1905.
[41] M. J. Bojdys, J. Jeromenok, A. Thomas, M. Antonietti, *Adv. Mater.* **2010**, *22*, 2202-2205.
[42] K. Wang, H. Huang, D. Liu, C. Wang, J. Li, C. Zhong, *Environ. Sci. Tech.* **2016**, *50*, 4869-4876.
[43] A. Bhunia, V. Vasylyeva, C. Janiak, *Chem. Comm.* **2013**, *49*, 3961-3963.
[44] A. Bhunia, D. Esquivel, S. Dey, R. Fernández-Terán, Y. Goto, S. Inagaki, P. Van Der Voort, C. Janiak, *J. Mater. Chem. A* **2016**, *4*, 13450-13457.
[45] G. Wang, K. Leus, S. Zhao, P. Van Der Voort, *ACS App. Mater. Interf.* **2018**, *10*, 1244-1249.
[46] L. M. Malard, M. A. Pimenta, G. Dresselhaus, M. S. Dresselhaus, *Phys. Rep.* **2009**, *473*, 51-87.
[47] J.-Y. Wu, M. G. Mohamed, S.-W. Kuo, *Poly. Chem.* **2017**, *8*, 5481-5489.
[48] Q. Wang, W. Xia, W. Guo, L. An, D. Xia, R. Zou, *Chem. Asian J.* **2013**, *8*, 1879-1885.
[49] P. Katekomol, J. Roeser, M. Bojdys, J. Weber, A. Thomas, *Chem. Mater.* **2013**, *25*, 1542-1548.
[50] S. Kandambeth, A. Mallick, B. Lukose, M. V. Mane, T. Heine, R. Banerjee, *J. Am. Chem. Soc.* **2012**, *134*, 19524-19527.
[51] X.-M. Hu, Q. Chen, Y.-C. Zhao, B. W. Laursen, B.-H. Han, *J. Mater. Chem. A* **2014**, *2*, 14201-14208.
[52] B. Marchon, J. Carrazza, H. Heinemann, G. A. Somorjai, *Carbon* **1988**, *26*, 507-514.
[53] L. Hao, S. Zhang, R. Liu, J. Ning, G. Zhang, L. Zhi, *Adv. Mater.* **2015**, *27*, 3190-3195.
[54] H. Wang, Z. Cheng, Y. Liao, J. Li, J. Weber, A. Thomas, C. F. J. Faul, *Chem. Mater.* **2017**, *29*, 4885-4893.
[55] M. Chaudhary, A. K. Nayak, R. Muhammad, D. Pradhan, P. Mohanty, *ACS Sustainable Chem. Eng.* **2018**, *6*, 5895-5902.
[56] S. N. Talapaneni, T. H. Hwang, S. H. Je, O. Buyukcakir, J. W. Choi, A. Coskun, *Angew. Chem. Int. Ed.* **2016**, *55*, 3106-3111.
[57] A. V. Bavykina, M. G. Goesten, F. Kapteijn, M. Makkee, J. Gascon, *ChemSusChem* **2015**, *8*, 809-812.
[58] A. F. M. El-Mahdy, C. Young, J. Kim, J. You, Y. Yamauchi, S.-W. Kuo, *ACS App. Mater. Interf.* **2019**, *11*, 9343-9354.
[59] M. M. M. Ahmed, T. Imae, J. P. Hill, Y. Yamauchi, K. Ariga, L. K. Shrestha, *Coll. Surf. A: Physicochem. Eng. Asp.* **2018**, *538*, 127-132.
[60] C. Gu, D. Liu, W. Huang, J. Liu, R. Yang, *Poly. Chem.* **2015**, *6*, 7410-7417.
[61] S. Himeno, T. Komatsu, S. Fujita, *J. Chem. Eng. Data* **2005**, *50*, 369-376.
[62] S. Keskin, T. M. van Heest, D. S. Sholl, *ChemSusChem* **2010**, *3*, 879-891.
[63] H. Gao, L. Ding, H. Bai, A. Liu, S. Li, L. Li, *J. Mater. Chem. A* **2016**, *4*, 16490-16498.
[64] A. F. M. EL-Mahdy, Y.-H. Hung, T. H. Mansoure, H. H. Yu,Y.-S. Hsu, K. W.C. Wu, S.W Kuo, *J. Taiwan Ins. Chem. Eng.* **2019,** 103, 199-208.

10.1002/cplu.201900635

WILEY-VCH



**Entry for the Table of Contents** (Please choose one layout)

# FULL PAPER

A series of bicarbazole-based covalent triazine frameworks (Car-CTFs) were synthesized under ionothermal conditions from Car-4CN in the presence of molten zinc chloride. Thermogravimetric and Brunauer–Emmett–Teller analyses revealed that these Car-CTFs possessed excellent thermal stabilities and high specific surface areas (ca. 1400 $m^2/g$). Exceptional electrochemical performance of Car-CFT-5-500 sample showed 545 F/g at 5 mV/s and highest $CO_2$ uptake capacities: 3.91 and 7.60 mmol/g at 298 and 273 K, respectively.

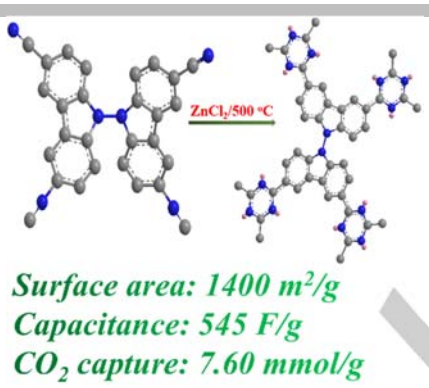


Mohamed Gamal Mohamed, Ahmed F. M. EL-Mahdy, Mahmoud M. M. Ahmed, and Shiao-Wei Kuo*

*Page No. – Page No.*

**Directly Synthesized Microporous Bicarbazole-Based Covalent Triazine Frameworks for High-Performance Energy Storage and Carbon Dioxide Uptake**